

A Microstructural Hyperelastic Model of Pulmonary Arteries Under Normo- and Hypertensive Conditions

YANHANG ZHANG,¹ MARTIN L. DUNN,¹ E. S. DREXLER,³ C. N. MCCOWAN,³ A. J. SLIFKA,³ D. D. IVY,²
and ROBIN SHANDAS^{1,2}

¹Department of Mechanical Engineering, University of Colorado, Boulder, Colorado 80309; ²The Children's Hospital of Denver, 1056 E. 19th Avenue, Denver, Colorado 80218; and ³NIST, Materials Reliability Division, 325 Broadway, Boulder, Colorado 80305

(Received 22 November 2004; accepted 21 April 2005)

Abstract—This work represents the first application of a statistical mechanics based microstructural orthotropic hyperelastic model to pulmonary artery mechanics under normotensive and hypertensive conditions. The model provides an analogy between the entangled network of long molecular chains and the structural protein framework seen in the medial layer, and relates the mechanical response at macro-level to the deformation (entropy change) of individual molecular chains at the micro-level. A finite element approach was adopted to implement the model. Material parameters were determined via comparing model output to measured pressure–stretch results from normotensive and hypertensive trunks and branches obtained from a rat model of pulmonary arterial hypertension. Results from this initial study show that this model appears reasonable for the study of hyperelastic and anisotropic pulmonary artery mechanics. Typical tangent modulus values ranged from 200 to 800 kPa for normotensive arteries—this increased to beyond 1 MPa for hypertensive vessels. Our study also provokes the hypothesis that increase of cross-linking density may be one mechanism by which the pulmonary artery stiffens in hypertension.

Keywords—Pulmonary arterial hypertension, Arterial biomechanics, Orthotropic hyperelasticity, Cross-linking, Tangent modulus, User material subroutine.

INTRODUCTION

Pulmonary arterial hypertension (PAH) is an important pathology within pediatric cardiovascular disease. In both primary (idiopathic) and secondary (congenital heart disease) forms, it presents increased hydraulic load on the right ventricle (RV), and if left untreated results in RV decompensation and subsequent failure. Primary PAH requires long-term treatment and careful serial monitoring, whereas secondary PAH is an important determinant of post-operative morbidity and mortality for repair of the congenital heart defect.¹⁹ For both etiologies, it is highly

important to accurately diagnose the severity of PAH and consequently the level of afterload imposed on the RV. Hemodynamic measurement of pulmonary vascular resistance (PVR) has been the clinical standard for evaluating pulmonary vascular function and, with the use of novel treatments such as low-dose inhaled nitric oxide and/or prostacyclin agents, evaluating reactivity of the pulmonary vascular bed by measuring changes in PVR upon clinical challenge. We have recently shown that measuring PVR alone may not provide a sufficiently comprehensive metric to evaluate pulmonary vascular reactivity and function; instead, obtaining upstream compliance information either indirectly by measuring the full input impedance of the vascular system, or directly through novel ultrasound tissue Doppler techniques, is needed to more fully quantify RV afterload.^{27,31} In fact, local compliance of the upstream pulmonary arteries can significantly modulate pulmonary vascular impedance.³¹

Understanding compliance effects is predicated upon elucidating the relationship between structure and mechanical function of the pulmonary arteries. Although it is well known clinically that the upstream pulmonary arteries “stiffen” with chronic PAH, there have been relatively few detailed mechanical studies of these arteries under normotensive and hypertensive conditions. Biological remodeling mechanisms of both downstream and upstream arteries have been studied for some time.^{14,23,26} Studying a rat model, Poiaian *et al.*²⁶ conclude that collagen and elastin, the primary structural proteins of the arterial wall, synthesize rapidly upon the initiation of hypoxia-induced PAH. Liu²³ suggests that altered tensile stress in the pulmonary artery wall plays a critical role in the initiation and regulation of the structural changes in the elastic laminae. Huang *et al.*¹⁴ has attempted to examine correlations between gene expression patterns for structural protein synthesis and tissue remodeling as well.

The relationship between biological remodeling and mechanical properties is obviously causal; nevertheless,

Address correspondence to Robin Shandas, PhD, Department of Mechanical Engineering, 427 UCB, University of Colorado, Boulder, Colorado 80309. Electronic mail: robin.shandas@colorado.edu

studies connecting micro-level changes with whole-artery mechanics are lacking. Instead, most investigators have relied on phenomenological approaches.^{6, 10, 13, 15, 16, 29, 30, 33} Strain energy functions of polynomial, exponential, and logarithmic forms are proposed in the literature to capture the hyperelastic response of arteries. Holzapfel *et al.*¹³ provide an excellent review and assessment of a range of two- and three-dimensional models. These strain energy functions utilize a continuum mechanics approach and are either invariants-based or principal-stretch based.¹⁷ Some strain energy functions⁶ focused mainly on capturing the hyperelastic behavior of arterial walls, with subsequent modifications regarding isotropy and heterogeneity. Holzapfel *et al.*¹³ proposed an orthotropic model that treats each layer of the artery as a fiber-reinforced composite. It assumes two families of fibers arranged helically within the arterial wall, characterized by two direction vectors, which are incorporated into the constitutive model.

Constitutive models based on non-Gaussian affine statistical characterization of a network of randomly oriented molecular chains are also proposed in the literature to provide microstructural information. Entropy-based constitutive laws are used to model the mechanical response of a single molecular chain. The essential idea is that the mechanical response of the material is due to an underlying molecular network structure, which relates applied deformation to the linking and geometric structure of individual molecular chains. Specific network models composed of three-chain,²⁰ four-chain,⁸ and eight-chain²⁻⁴ unit elements are proposed to model a network of molecular chains to obtain a continuum behavior. Boyce and Arruda⁵ reviewed several recent and classic statistical mechanics and continuum mechanics based models. To the best of our knowledge, there has been no study applying the statistical mechanics based model to artery wall mechanics.

In this study, we develop a microstructural approach to the study of pulmonary artery behavior using a statistical mechanics methodology originally developed by Arruda and Boyce² for isotropic hyperelasticity and modified by Bischoff *et al.*^{3, 4} to incorporate orthotropy. The eight-chain element was selected as the basic unit; these can have different dimensions in the three orthogonal material directions and in this manner, the response of the unit element is made orthotropic. The primary aim of this study was to adapt the general statistical mechanics based microstructural model to the specific study of pulmonary artery behavior. Secondary aims were to use preliminary biomechanical test data from a rat model of PAH to determine model parameters for the medial layer of the trunk and main branch pulmonary arteries with and without PAH, and to begin developing hypotheses linking microstructural changes with PAH.

MATERIALS AND METHODS

Histological/Microstructural Basis of the Model

Figure 1 shows a general schematic of the artery wall, consisting of the adventitia, composed of connective tissue components, with collagen dominating the structural protein components; the media, consisting of elastin-based laminae surrounded by extra-cellular matrix and smooth muscle cells; and the innermost intima, which is an epithelial monolayer of endothelial cells and which does not contribute significantly to the mechanical behavior. In this study, we focused our modeling efforts on the medial layer for several reasons. First, companion experimental studies on rat pulmonary arteries were performed with the adventitial layer removed; second, the elastin-configuration of the medial layer provides a reasonably direct analogy with the molecular microstructure of the model; and third, we did not wish to unnecessarily complicate the model for this initial investigation. Subsequent models are being developed to allow inclusion of both elastin-like and collagen-like molecular networks and thereby incorporate the adventitial layer as well. For the medial layer, then, the microstructure can be represented as a tangled molecular network with individual molecular fibers connected to each other via cross-linking and entanglement. A representation of a typical unit element within the model based on this microstructural idea is also shown in Fig. 1. Note that the eight-chain network model does not represent the actual organization/alignment of the protein fibers in the medial layer and the molecular chains within the unit element are not intended to represent with anatomic accuracy the molecular structure of an elastin molecule; instead, the molecular chain represents the *functional equivalent* in a mechanical sense of the molecular fiber network found in the medial layer.³³ When the arteries

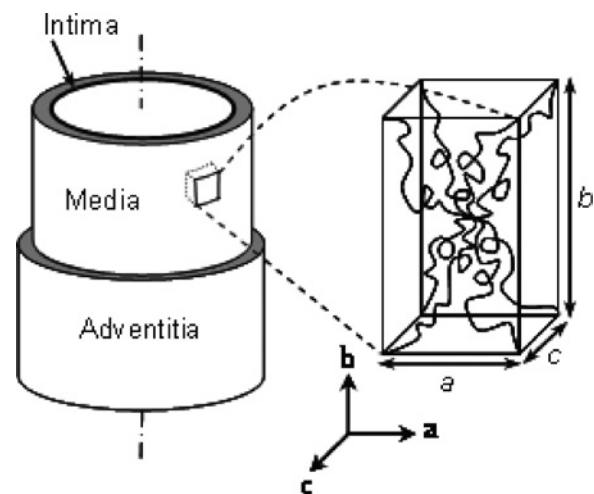


FIGURE 1. Schematic of the artery wall and the 8-chain orthotropic unit element used to model the orthotropic behavior of the network structure in the medial layer.

are stretched, the constituents of this network structure, and consequently the individual element, will redistribute.⁹ The overall macro-level mechanics thus needs to be represented as both anisotropic and hyperelastic.

Mechanical Basis of the Model

The model is three-dimensional, orthotropic, and hyperelastic and is developed from a general model described by Bischoff *et al.*^{3,4} to which the reader is referred for greater detail regarding the development of the constitutive equations. We describe basic aspects here. As shown in Fig. 1, the fundamental component of the network structure of the artery wall in the model is a unit element, which is characterized by three orthogonal unit vectors, **a**, **b**, and **c**, representing principal material directions. In each unit element, eight molecular chains are situated along the diagonals of the unit element and linked together at the center of the element. The chains deform with element deformation. The dimensions of the unit element along each orthogonal direction can vary, which in turn changes the response of the element (i.e., the element is orthotropic). As the material deforms, each unit element, and thus the eight constituent molecular chains, will be deformed. Each chain is treated as a macromolecule, which is modeled as a freely joined chain. The strain energy of each unit element is associated with the entropy change of the chains. The overall energy function for the material is then a summation of all unit element energies, and can be written as^{3,4}

$$w = w_0 + \frac{nk\Theta}{4} \left[N \sum_{i=1}^4 \left(\frac{\rho^{(i)}}{N} \beta_\rho^{(i)} + \ln \frac{\beta_\rho^{(i)}}{\sinh \beta_\rho^{(i)}} \right) - \frac{\beta_p}{\sqrt{N}} \ln (\lambda_a^2 \lambda_b^2 \lambda_c^2) \right] + B [\cosh(J - 1) - 1] \quad (1)$$

where w is the overall energy, w_0 is a constant, B is a parameter that controls the bulk compressibility, and J is the volume ratio. Parameters a , b , and c are normalized dimensions along the principal material directions, and λ_a , λ_b , and λ_c are stretches along these directions. $N = \frac{a^2 + b^2 + c^2}{4}$ is the number of rigid links within each individual chain. \sqrt{N} defines the extensibility of the chain, i.e., as the chain stretch approaches \sqrt{N} , the stiffness increases dramatically, thereby resulting in the strain-stiffening response of the macromolecule. $\rho^{(i)}$ are the normalized deformed lengths of the constituent chains in the unit element. $\beta_\rho^{(i)} = \ell^{-1}(\rho^{(i)}/N)$, and $\ell(x) = \coth x - 1/x$ is the Langevin function. $\beta_p = \ell^{-1}(p/N)$, where $p = \frac{1}{2}\sqrt{a^2 + b^2 + c^2}$ is the initial normalized length of each chain. Parameter n is the chain density per unit volume; $k (= 1.38 \times 10^{-23} \text{ J/K})$ is Boltzmann's constant; $\Theta = 298 \text{ K}$ is absolute temperature. Note that $nk\Theta$ defines the initial stiffness, and B is signifi-

cantly greater than $nk\Theta$ to model the nearly incompressible material behavior.

Input Material Parameters for the Model

It is useful to relate the input parameters of the model to the physiological situation. The input material parameters for the model are normalized dimensions of the unit element: a , b , and c ; and the chain density per unit volume: n . Note that the dimensions of the unit element and the chain density are related in the model; however, we discuss them separately here to separate their functional mechanical effects. The a and b directions are aligned along the circumferential and longitudinal coordinates of the artery, respectively. The relative values of a , b and c , then, provide information on the degree of orthotropy that exists in the artery wall. If $a = b = c$, the artery wall is isotropic. For the pulmonary artery, we initially set a , $b > c$ to simulate the primary distribution patterns of the fibers reinforcing the wall. The overall behavior of the artery can thus be classified as cylindrically orthotropic. Quantitative three-dimensional micro-histology data of the distribution of component molecular structures within the media layer would help determine parameters a , b , and c in a unique sense. However, these data are not yet available at this dimensional level in the literature for pulmonary arteries, and to the best of our knowledge, there is no study on the stiffness of the pulmonary arteries in the thickness direction. Our initial assumptions of a , $b > c$ is consistent with the study by Holzapfel *et al.*,¹³ where the medial and adventitial layers are modeled as fiber-reinforced material with no fiber contribution in the thickness direction. $N = \frac{a^2 + b^2 + c^2}{4}$ is related to the molecular chain length between the two cross-links at micro-level, and the extensibility of the material at macro-level. A less extensible material will be expected to be more cross-linked and thus have a smaller N . The molecular chain density per unit volume, n , is related to the initial stiffness of the material.

Finite Element Implementation

We take a finite element approach to solve the complex set of equations for the deformation of an orthotropic hyperelastic solid of a specified geometry subjected to prescribed loads and boundary conditions. In general, both geometric (large deformation) and material (stress-strain relationships) nonlinearities are present. The model was implemented in a commercial finite element simulation program.¹¹ A customized user material subroutine was created to prepare the problem for finite-element solution, which involves determination of the Cauchy stress and elasticity tensor in the deformed configuration. From the strain energy function in Eq. (1), the second Piola-Kirchhoff stress tensor can be calculated as $\mathbf{S} = 2 \frac{\partial w}{\partial \mathbf{C}}$, where \mathbf{C} is the

right Cauchy–Green tensor. The tensor form of the second Piola–Kirchoff stress is

$$\mathbf{S} = \frac{nk\Theta}{4} \left[\sum_{i=1}^4 \frac{\mathbf{P}^{(i)}\mathbf{P}^{(i)T}}{\rho^{(i)}} \beta_{\rho}^{(i)} - \frac{\beta_p}{\sqrt{N}} \left(\frac{a^2}{\lambda_a^2} \mathbf{aa}^T + \frac{b^2}{\lambda_b^2} \mathbf{bb}^T + \frac{c^2}{\lambda_c^2} \mathbf{cc}^T \right) \right] + BJC^{-1} \sinh(J - 1) \tag{2}$$

where $\mathbf{P}^{(i)}$ is the normalized chain vector describing the i th undeformed chain.^{3,4} The elasticity tensor in the reference configuration, defined as $\mathbf{H} = 2 \frac{\partial \mathbf{S}}{\partial \mathbf{C}}$, can then be calculated from Eq. (2) as

$$\mathbf{H} = \frac{nk\Theta}{4} \left\{ \sum_{i=1}^4 \left[\frac{1}{N(\rho^{(i)})^2 (-\csc h^2 \beta_{\rho}^{(i)} + 1/(\beta_{\rho}^{(i)})^2)} - \frac{\beta_{\rho}^{(i)}}{(\rho^{(i)})^3} \right] \mathbf{P}^{(i)}\mathbf{P}^{(i)T} \otimes \mathbf{P}^{(i)}\mathbf{P}^{(i)T} + \frac{2\beta_p}{\sqrt{N}} \left(\frac{a^2}{\lambda_a^4} \mathbf{aa}^T \otimes \mathbf{aa}^T + \frac{b^2}{\lambda_b^4} \mathbf{bb}^T \otimes \mathbf{bb}^T + \frac{c^2}{\lambda_c^4} \mathbf{cc}^T \otimes \mathbf{cc}^T \right) \right\} + BJ[\sinh(J - 1) + J \cosh(J - 1)]\mathbf{C}^{-1} \otimes \mathbf{C}^{-1} + 2BJ \sinh(J - 1) \frac{\partial \mathbf{C}^{-1}}{\partial \mathbf{C}} \tag{3}$$

The Cauchy stress and elasticity tensor in the deformed configuration can then be achieved by applying a push forward operation¹² on Eqs. (2) and (3). The custom material subroutine and subsequent finite element solutions were tested for robustness prior to studying the pulmonary artery configuration by performing simple tests and comparing the results with those by Bischoff *et al.*⁴ These revealed minimal differences.

Shell elements were used for modeling because such elements resemble the geometric characteristics of the artery wall where the dimension in the thickness direction is much smaller than that along the other two directions. Furthermore, the inherent plane-stress assumption for shell elements greatly simplifies the equations and facilitates solution convergence for this nonlinear problem. We use general-purpose shell elements with reduced integration (S4R) in our model.

The user material subroutine needs to be compatible with the plane-stress configuration to incorporate shell elements. Stress element output for shell elements contains only three components: σ_{11} , σ_{22} , and τ_{12} . Stress components σ_{33} , τ_{13} , and τ_{23} are assumed to be zero. Stress and strain in plane-stress problems are related via the *reduced stiffness matrix*.¹⁸ When shell elements are used together with the user material subroutine, transverse shear stiffness is required in the input file. We estimated it at the initial state with no deformation. Our tests have shown that varying the

transverse shear stiffness does not change the result, but affects the solution convergence rate.

The geometric configuration of the finite element model is shown in Fig. 2; it models a bubble inflation test of an arterial wall section, which was the experimental protocol performed as part of a prior study examining pressure–stretch characteristics of pulmonary arteries.⁷ We decided to simulate the same conditions as in the experimental test to determine the material parameters and thus validate the finite element model. However, note that once the model has been validated, the model geometry can be changed easily to represent a branching tube network, which allows subsequent simulations to be run and predictions obtained on realistic vascular geometry. We have an ongoing study to obtain patient-specific three-dimensional pulmonary vascular geometry and subsequently plan on incorporating this statistical mechanics based microstructural model to patient-specific anatomy.²¹ This is one of the strengths of the finite element method.

The model resembles a section of the pulmonary artery wall that has been dissected away and mounted *in vitro* within an inflation chamber for mechanical testing. The experimental test configuration consisted of a circular disk-shaped section of the artery subject to varying pressure loads. This is commonly referred to as a bubble or membrane-inflation test.¹⁷ Based on symmetry

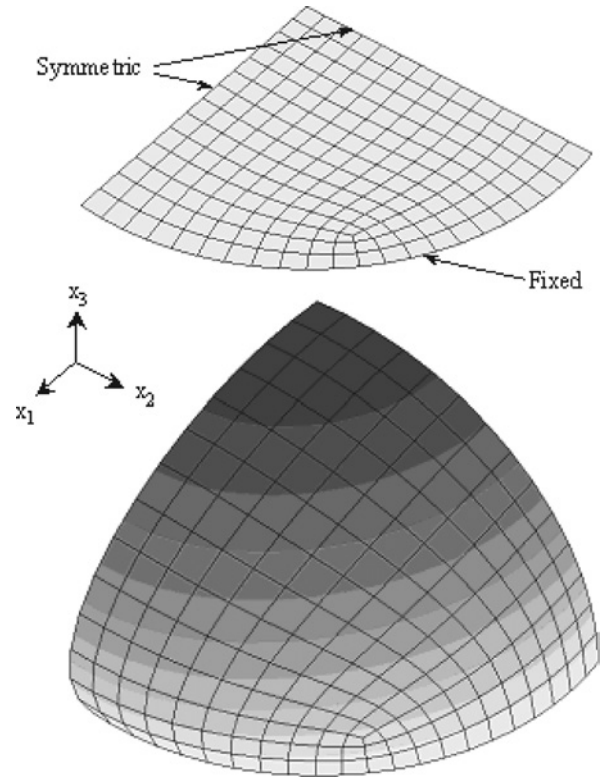


FIGURE 2. Configuration of the finite element model: undeformed (above) with boundary conditions and deformed (below) with each contour band representing a displacement of 0.094 mm in the x_3 direction.

considerations, only a quarter of the bubble with symmetric boundary conditions was modeled in the finite element study. The displacements were fixed at the edge of the bubble. Typical finite element meshes for the bubble contained elements with a characteristic dimension of about 0.08 mm, a size that was chosen after a mesh-validation study examining the tradeoffs between convergence rates and mesh resolution.

Experimental Protocol

Application of the finite element results was performed using data from an earlier preliminary experimental study of normotensive and hypertensive (ET-B receptor deficient hypoxic) Long-Evans rat models. The experimental work has been published elsewhere;⁷ only basic aspects are provided here. Figure 3(a) provides a schematic of the test fixture. A bubble inflation test setup was custom-designed to study disk-shaped specimens from the arterial wall of the trunk and main right and left branches. The adventitial layer was carefully removed, and longitudinal and transverse directions were marked on the disk specimen prior to measurements. Micro-histology of the specimens pre- and post-removal of the adventitia confirmed that the medial layer was minimally affected (i.e., lamellar layers were maintained, medial thickness did not change, etc.). The specimen was pressurized using isotonic buffered saline, and the shape of the bubble as a function of pressure was captured by cameras located at different angles. The arc

length was then determined to calculate stretch and strain. Figure 3(b) shows the side view image of an inflated specimen. Average stretch (λ) at each pressure is calculated as the arch length (l) of the bubble divided by the diameter of the aperture ($l_0 = 2.32$ mm) through which the specimen is inflated: $\lambda = l/l_0$. The knock-out rats spent 3–4 weeks (mean: 24 days) in a hypobaric chamber to induce the development of hypoxic PAH. The oxygen concentration in the hypobaric chamber was equivalent to that at an altitude of 5182 m. The body weights of the rats were 300–400 g. All the tests were performed within 24 h after the rats were sacrificed. The specimen was preconditioned with the pressure cycled 5 times from 0 to 3.45 kPa prior to the test.

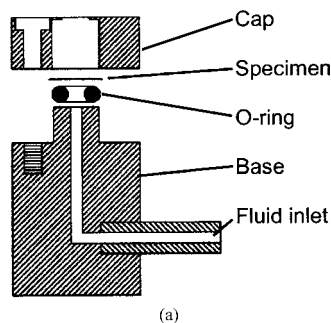
RESULTS

General Experimental Observations

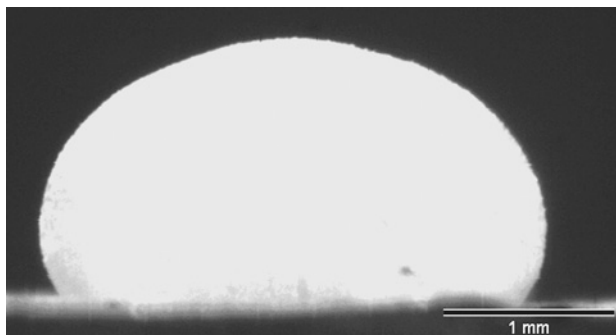
Representative experimental results will be shown together with the finite element simulations. Detailed experimental results can be found elsewhere;⁷ to focus on model issues, only general observations are presented here. The presence of different stretch values in the two directions at the same pressure indicates anisotropy within the tissue, especially at high pressure. In general, the trunk is stiffer in the circumferential direction than the longitudinal direction. Interestingly, the anisotropy in the main branches manifests in opposite fashion to that found in the trunks: for both main branches, the longitudinal direction is stiffer than the circumferential direction while the opposite is true for the trunk. Animal-to-animal variability is significant, especially at high pressure. At a pressure of 15 kPa (112.5 mmHg), stretch for normotensive trunks can vary from 1.28 to 1.7. There appears to be a greater extent of anisotropy for the normotensive branches than for the normotensive trunk although further testing is required for a definitive answer. At a pressure of 15 kPa, the stretch for hypertensive trunks and main branches is in the range of 1.15–1.32. Even with this large range of values, it is clear that the lower values of stretch for hypertensive pulmonary arteries indicate decreased extensibility compared with the normotensive case.

Finite Element Simulations

The first part of the finite element simulation involved extracting material parameters that matched the experimental data. In the determination of the material parameters, we imposed an initial boundary criterion on the relative magnitude of material parameter c to those of a and b . We assumed $a, b > c$ and c is about 70–80% of the smaller of a and b , i.e., the artery is stiffer in the longitudinal and circumferential directions than in the thickness direction. This assumption together with the anisotropy and extensibility information from each set of pressure–stretch measurements, and the initial stiffness of the material, will determine the particular



(a)



(b)

FIGURE 3. (a) Schematic of the bubble test fixture, (b) side-view image of the inflated specimen.

set of material parameters (a , b , c , and n) for each set of experimental data.

Pressure–stretch results from the simulation were compared to the experimental data and material parameters were adjusted for a subsequent run, until experimental and simulated pressure–stretch results matched. The maximum difference between model and experimental results was 3.6%. The process of matching the simulations to the measurements allowed us not only to determine the particular values of the model parameters to match experimental data but also to relate essential aspects of the molecular network (the unit element configuration) to the normotensive and hypertensive data by examining how material parameters changed with hypertension. Pressure–stretch data from four normotensive and four hypertensive animals were used in the finite element simulation for extracting the material parameters. The material parameters obtained in this way and corresponding measured thickness for the trunks and main branches are summarized in Table 1.

Figure 4 shows representative pressure versus stretch results obtained from both the experimental tests and finite element simulations for one normotensive and one hypoxic hypertensive rat. For each rat, results from trunk and main branches are shown. Squares are measurements and solid lines are simulations. Results from finite element simula-

tions were based on the material parameters summarized in Table 1.

Once the model parameters have been determined, the finite element approach allows study of the problem in much greater detail than can be done experimentally. For example, we can extract the average stress as a function of stretch in both longitudinal and circumferential directions. The average stress provides an approximation of local stress over the membrane and is a useful quantity to report when local stresses vary both through the thickness of the membrane and over the in-plane directions.³⁴ From the average stress, we can extract the biaxial tangent modulus by differentiation of the average stress–stretch curve under equi-biaxial plane-stress assumptions, $E_t/(1 - \nu) \approx d\sigma/d\lambda$, where ν is Poisson’s ratio, and E_t is the tangent modulus. We assume $\nu \approx 0.5$ for nearly incompressible material, so that E_t can be estimated as $E_t \approx \frac{1}{2}d\sigma/d\lambda$. Exponential functions were fitted to the $\sigma - \lambda$ curves and then differentiated to obtain E_t in the longitudinal and circumferential directions. The tangent modulus provides a measure of material stiffness at different stress/strain configurations.

Figure 5 shows the average stress in the longitudinal and circumferential directions of the left main branches from finite element simulations for the rats in Fig. 4. For these two left main branches, average stress in the longitudinal

TABLE 1. Animal number, artery and thickness measurements from the experimental data used to extract model parameters for the finite element simulations, as well as the material parameters obtained from the finite element simulations are shown here. Both normotensive and hypertensive conditions were modeled.

		Thickness (mm)	n (1/mm ³)	Material parameters			
				a	b	c	N
Normotensive							
2101	Trunk	0.1256	6.5×10^{15}	2.21	1.36	1.13	2
	Left	0.0711	7.4×10^{15}	1.85	2.08	1.5	2.5
1594	Trunk	0.1651	1×10^{16}	2.6	1.95	1.62	3.3
	Left	0.0839	8.7×10^{15}	1.3	2.39	1	2.1
	Right	0.0711	1.43×10^{16}	1.36	2.5	1.13	2.35
9373	Right	0.1505	7×10^{15}	1.3	2.3	1	2
8271	Right	0.1951	2×10^{15}	1.58	2.15	1.3	2.2
Average		0.1239	7.99×10^{15}				2.35
±SD		±0.0488	± 3.74×10^{15}				±0.46
Hypoxic hypertensive							
1592	Trunk	0.0996	2×10^{16}	2.48	1.51	1.26	2.5
	Left	0.1117	1.58×10^{15}	1.01	1.84	0.79	1.26
	Right	0.2413	1.68×10^{15}	2.01	1.1	0.86	1.5
1385	Trunk	0.1473	1.4×10^{16}	1.83	1.83	1.3	2.1
	Left	0.1346	1.5×10^{15}	0.98	1.8	0.77	1.2
	Right	0.1117	1.55×10^{16}	1.74	1.74	1.4	2
4234	Trunk	0.1562	1.28×10^{16}	2.68	1.28	1.08	2.5
	Left	0.2377	1.55×10^{15}	0.77	2.233	0.65	1.5
	Right	0.143	1.30×10^{15}	0.71	2.0435	0.6	1.26
4235	Left	0.1549	1.20×10^{15}	0.65	2.077	0.55	1.26
	Right	0.1471	1.15×10^{15}	0.71	2.0435	0.6	1.26
Average		0.1532	6.57×10^{15}				1.67
±SD		±0.0466	± 7.35×10^{15}				±0.51

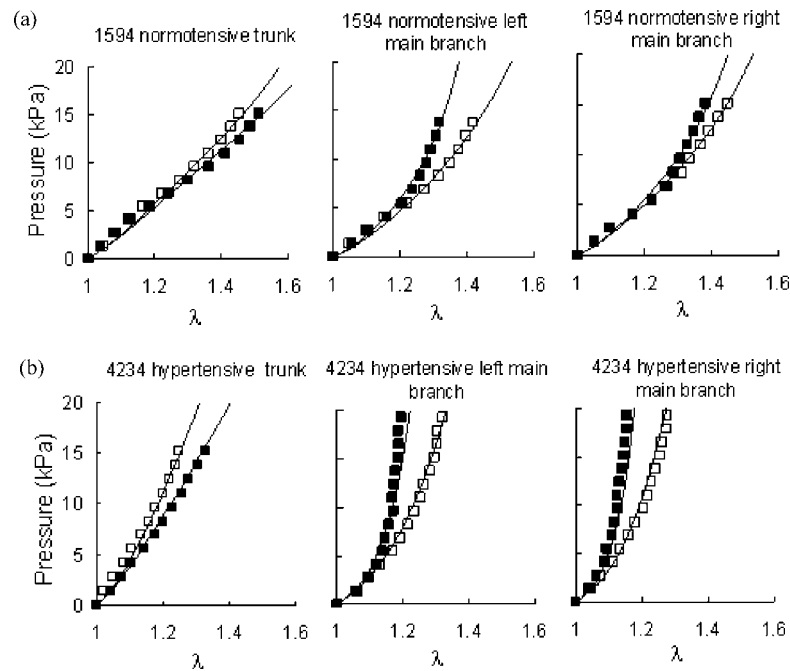


FIGURE 4. Representative measured (squares) and predicted (solid lines) pressure vs. stretch in longitudinal and circumferential directions of (a) the normotensive, and (b) the hypertensive pulmonary trunk and main branches. Open squares are measurements in circumferential direction and filled squares are measurements in longitudinal direction. Material parameters for the finite element simulation are summarized in Table 1.

direction is higher than that in the circumferential direction. Due to the early strain stiffening effect and thus increase in stiffness for the hypertensive left main branches at similar stretch values, the average stresses in the hypertensive arteries shown in Fig. 5(b) are comparable with those in the normotensive arteries shown in Fig. 5(a).

Figure 6 shows the tangent modulus versus stretch in both the longitudinal and circumferential directions for four normotensive and hypertensive left main branches. For normotensive left main branches, the initial tangent modulus is between 0.04 and 0.05 MPa in circumferential direction, and between 0.07 and 0.17 MPa in longi-

nal direction. The initial tangent modulus for hypertensive left main branches falls in the same ranges as that found in the normotensive cases in both directions. However, as stretch increases, the hypertensive left branches exhibit earlier strain stiffening in the longitudinal direction, where after a stretch of about 1.1 the tangent modulus increases dramatically. The tangent modulus for right main branches possesses similar behaviors for both the normotensive and hypertensive arteries (results not shown). The trunks are

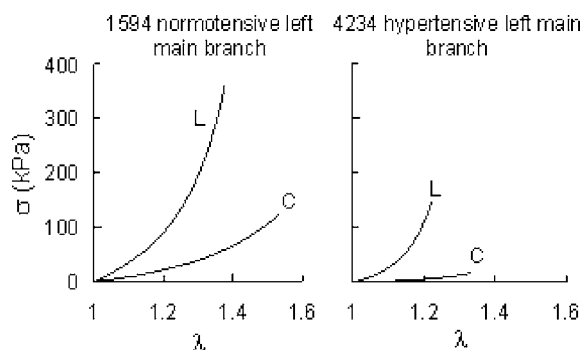


FIGURE 5. Representative predicted average stress vs. stretch in longitudinal (L) and circumferential (C) directions of (a) normotensive and (b) hypertensive left main branches.

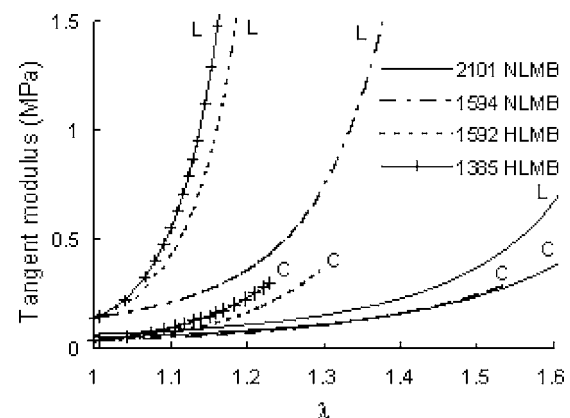


FIGURE 6. Predicted tangent modulus vs. stretch in longitudinal (L) and circumferential (C) directions of two normotensive left main branches (NLMBs) and two hypertensive left main branches (HLMBs) shown in Table 1.

stiffer in the circumferential direction than in the longitudinal directions. There is an increase in the initial tangent modulus, but there is no significant strain stiffening effect for hypertensive trunks.

Sensitivity of the Individual Material Parameters

Although a comprehensive examination of material parameter sensitivity is beyond the scope of this paper, we performed a limited study on the effect of individual material parameters in predicting the pressure–stretch relationship. Specifically, the effects of chain density per unit volume, chain extensibility, and the stiffness in the thickness direction on the pressure–stretch prediction were studied. Figure 7(a) shows results on the effect of chain density per unit volume. One group of the material parameters from Table 1, $n = 2 \times 10^{15}$, $a = 1.58$, $b = 2.15$, $c = 1.3$, and $N = 2.2$, were used in the simulation. The chain density per unit volume is increased from n , to $2n$, and $4n$. Figure 7(b) shows the result on the effect of chain extensibility. The material parameters a , b , and c are fixed to be $a = b = c = \sqrt{\frac{4N}{3}}$ (the material is isotropic in this case) to facilitate comparison. Material parameter N values used were 1.8, 2, and 2.2. Figure 7(c) shows results on the effect of the stiffness in the thickness direction. To study this, material parameter $N = \frac{a^2+b^2+c^2}{4}$ which is related to the chain length and also the chain extensibility, is fixed to be 2.2, and parameters a and b are set to be equal, i.e., $a = b$ (the material is transversely isotropic in this case) to facilitate comparison. The ratios of c/a used were 0.8, 0.9, and 1.

DISCUSSION

To the best of our knowledge, this paper represents the first study to develop and implement a statistical mechanics based orthotropic hyperelastic microstructural model for pulmonary artery mechanics under normotensive and hypertensive states. We have shown that an orthotropic eight-chain hyperelastic model is capable of resolving the experimentally measured pressure–stretch data from normotensive and hypertensive rat pulmonary trunks and main branches. The model allowed further investigation into average stresses and perhaps more importantly the tangent modulus for these arteries as a function of stretch. The application of such a model to the study of pulmonary artery mechanics allows links to be studied between unit element characteristics and corresponding macro-level behavior. Adjusting material parameters in the model to match normotensive and hypertensive data also provide initial clues regarding how hypertension may affect intra-molecular linking and thus alter arterial mechanics. Lastly, the model can be applied to patient-specific three-dimensional vascular anatomy data to obtain detailed mechanical predictions of pulmonary artery behavior, which should be useful in

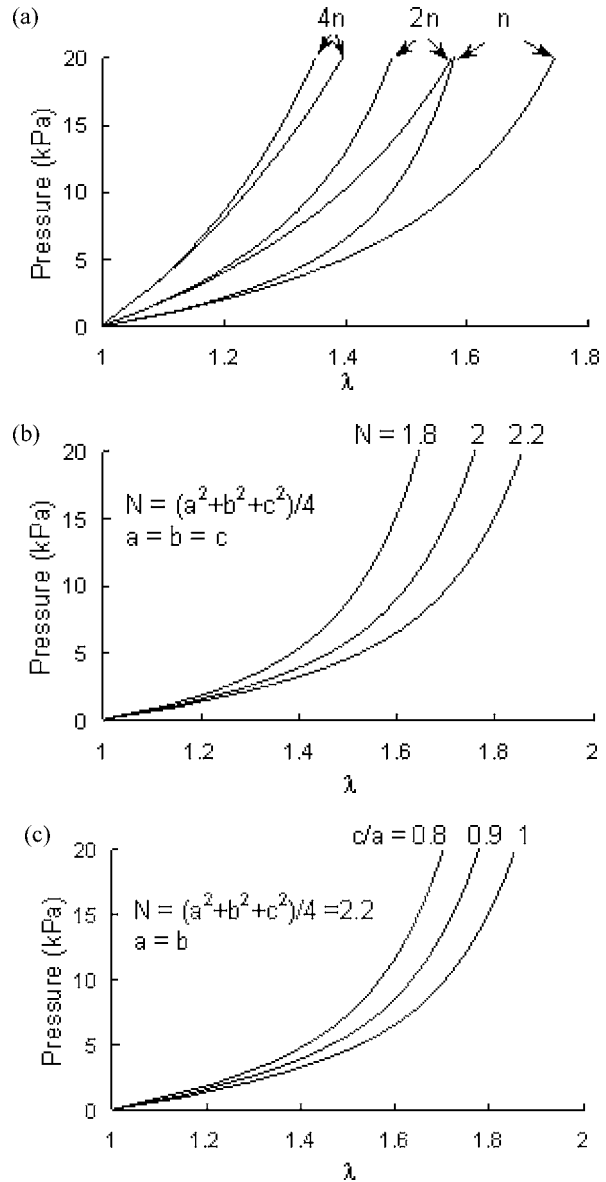


FIGURE 7. Effect of individual material parameters in predicting the pressure–stretch relationship. Material parameter $n = 2 \times 10^{15}$ ($1/\text{mm}^3$) for all the simulations. (a) Effect of chain density per unit volume; material parameters $a = 1.58$, $b = 2.15$, $c = 1.3$, and $N = 2.2$. The chain density per unit volume is increased from n , to $2n$, and $4n$. (b) Effect of chain extensibility. Material parameter N is varied ($= 1.8, 2$, and 2.2); $a = b = c = \sqrt{4N/3}$. (c) Effect of the stiffness in the thickness direction. $N = 2.2$, $a = b$, the ratio of c/a is varied ($= 0.8, 0.9$, and 1).

following disease progression, especially regarding the initiation and effects of arterial remodeling in PAH, and in more accurately estimating pulmonary vascular reactivity in patients undergoing pulmonary vasodilator challenge as is routinely done at our institution.³¹

The extent of anisotropy for one animal is within the animal-to-animal variability we found in the experimental pressure–stretch measurements, indicating that variation in

macro-level anisotropy is likely within the range of biological variability. Many modeling studies assume the artery is isotropic. Although this might be sufficient for certain applications such as where bulk material properties are to be studied, it ignores the inherent information associated with the orthotropic nature of the arterial wall. As shown in Fig. 5, when the strain stiffening effect manifests, the stress increases substantially. As our studies show, this phenomenon is in general more pronounced in one direction than in the other, with the result that wall stresses in the direction with increased strain stiffening can be much higher than the wall stresses in the other direction. Physiologically, this distinction is important in PAH since fibroblasts, smooth muscle cells and a variety of precursor cells may alter function based on local material stresses and strains.¹ Similarly, the tangent modulus in Fig. 6 can also differ appreciably in the two directions, especially after the strain stiffening point.

In general, the circumferential tangent modulus for the trunks was higher than the longitudinal tangent modulus, indicating greater resistance to stretch for arterial expansion radially than longitudinally. Strain stiffening was found to manifest earlier for the main branch arteries than for the trunks. Typical tangent modulus values for trunk and branch arteries were in the 200–800 kPa range, while hypertensive conditions increased the values to beyond 1 MPa, especially for the left branch at very high (>20 kPa) pressures. The manifestation of the strain-stiffening effect at a lower stretch value may thus be an important marker of early structural modulation. For example, the initial tangent modulus values for normotensive and hypertensive left main branches were about the same. However, the strain stiffening effect for the hypertensive animals manifests at a stretch of only 1.1, resulting in a dramatic increase in the longitudinal tangent modulus. The circumferential tangent modulus increased as well, but without a clear demarcation of strain stiffening, implying greater tensile resistance by wall fibers for axial deformation.

Reasons for the opposing anisotropic trends found in the trunks versus main branches are unclear. In general, there have not been many studies on the anisotropic mechanical properties of pulmonary arteries. Huang *et al.*¹⁵ studied changes of incremental Young's modulus of rat left main branch in circumferential and longitudinal directions over a 24 h period of hypoxic breathing. The perturbation of stresses and strains were related by linear, anisotropic, tensor equations involving three elastic constants: the incremental Young's modulus in the circumferential direction, that in the longitudinal direction, and the cross modulus. They found higher circumferential Young's modulus (0.164–0.187 MPa) than longitudinal Young's modulus (0.064–0.092 MPa) in left main branches. Our experimental results show that the longitudinal direction is stiffer than the circumferential direction in left main branches for all the normotensive and hypertensive rats

that exhibit anisotropic material behavior. The reason for this contradiction might be that only the medial layer is included in our study. Adventitial reinforcement through increased levels of fibroblast activity may alter this trend, and will need to be examined in future studies.

Our study sheds light on the relationship between the change in artery mechanics and the potential change in microstructure for PAH. Our results suggest that there is no significant change in the chain density per unit volume (from a mean \pm SD of $7.99 \times 10^{15} \pm 3.74 \times 10^{15}$ to $6.57 \times 10^{15} \pm 7.35 \times 10^{15}$, $p = 0.60$); however, chain extensibility decreased significantly (from a mean \pm SD of 2.35 ± 0.46 to 1.67 ± 0.51 , $p = 0.01$) for hypertensive arteries. Although studies utilizing larger numbers of animals are needed to fully document these changes, these results are consistent with biological observations and provoke interesting hypotheses for future studies. Rapid synthesis of collagen and elastin during hypoxic PAH has been found by many biological studies.^{22,24,26} Liu²² found proliferation of smooth muscle cells as well as excessive production of collagen fibers after 2 days of hypoxia in the medial layer of the right hilar pulmonary arteries. Meyrick and Reid²⁴ studied the medial and adventitial layer separately in the rat hilar intrapulmonary artery. They found that hypoxia caused significant thickening of the medial layers due to hypertrophy of smooth muscle cells, extracellular connective tissue, collagen fibers, and elastin. Our experimental studies also show a slight, albeit statistically insignificant, increase in the thickness of the medial layer (from a mean \pm SD of 0.1239 ± 0.0488 mm to 0.1532 ± 0.0466 mm, $p = 0.23$) of pulmonary arteries with PAH. In a study of rats with hypoxic PAH, Poiani *et al.*²⁶ found that there was no change in the proportion of collagen and elastin relative to the increased mass of the hypertensive vessel. The proportional increase in structural proteins of hypertensive vessel, collagen and elastin, is consistent with our result of no significant change in the chain density per unit volume. The decrease in chain extensibility indicates that the mean spacing between molecular links has decreased in the hypertensive case, and implies greater degree of molecular cross-linking within, for example, elastin to both other elastin molecules and/or to other structural protein fibers found in the medial extracellular matrix. Although no biological studies appear to have been done to examine cross-linking of pulmonary arteries in PAH, there have been similar studies for systemic hypertension³² that suggest that the additional elastin neither thicken the existing elastic lamina nor produce new elastic lamina, but is deposited in interlamellar islands and result in microstructural changes in the architecture. A few authors have also suggested that the degree of collagen cross-linking is a predictor of stiffness in the myocardium.^{22,25,28} Results from these studies fit with our prediction of increased molecular linking albeit in the medial layer and suggest examination

of molecular cross-linking as a potential mechanism by which cardiovascular soft-tissue increases material stiffness.

To best understand how material parameters may affect ultimate mechanical response for such a complex constitutive material law, it is important to understand the effect of the individual material parameters in predicting the pressure–stretch response. Chain density plays a role in determining the initial slope of the pressure–stretch curve. For orthotropic materials with constant pressure loading, as chain density increases both the stretch and anisotropy decrease. Chain extensibility plays a role in determining where the strain stiffening starts. The effect of the stiffness in the thickness direction relative to the stiffness in the in-plane direction, c/a , on the in-plane mechanical response is also important and needs to be understood to more accurately interpret the microstructural indication of the material parameters. Figure 7(c) shows that for fixed chain extensibility, decreasing the ratio of c/a can cause a similar effect on the pressure–stretch curve to that seen by decreasing the chain extensibility shown in Fig. 7(b).

It is important to recognize several limitations in our study. The experimental results were from a small group of animals. The intent of this paper was to develop and perform initial validation of a novel model. The large variation in mechanical properties seen in the experimental data and the fact that only limited number of animals were used precludes comprehensive statistical analysis from being done at this point. In this respect, additional experimental data will be needed to obtain the full range of variation in material parameters between normotensive and hypertensive conditions. The actual alignment and mechanical properties of the elastic and collagen fibers are not taken into account in the current model. However, the model is an advance over prior models that have used macro-level features and we provide it within this context. Subsequent work advancing this model to include specific structure–function relationships of single elastin/fibrillin and collagen molecules is planned; however, this requires *a-priori* knowledge of single molecule mechanics, which is currently unavailable. Further studies relating microbiological observations of single fibers and indeed single structural proteins within the arterial wall to mechanical statistical mechanics based microstructural models would thus appear warranted.

We conclude that a statistical mechanics-based microstructural model of pulmonary artery mechanics appears to be a reasonable means of studying normotensive and hypertensive arteries and provides clues regarding the relationship between microstructural properties and macro-level behavior. Further development of this model will include a separate unit element for the adventitial layer and linking of the existing generic molecular chain properties to specific mechanical properties seen for elastin and collagen molecules. Lastly, the model is also being merged with three-dimensional clinical images of the pulmonary

vasculature from PAH patients to study arterial mechanics on a patient-specific level.

ACKNOWLEDGMENTS

This work was supported in part through grants from the NIH (HL 072738 and HL 067393). We also wish to thank Dr Neil Davie from UCHSC for valuable discussion regarding the micro-biology of the pulmonary arteries, Dr H. Jerry Qi from University of Colorado at Boulder, and Dr Jeffrey E. Bischoff from South Carolina University for discussion regarding the statistical mechanics based microstructural model. R.S. would like to dedicate this paper to Prof John T. (Jack) Reeves.

REFERENCES

- ¹Anthony, G., M. D. Durmowicz, and K. R. Stenmark. Mechanisms of structural remodeling in chronic pulmonary hypertension. *Pediatr. Rev.* 20:e91–e102, 1999.
- ²Arruda, E. M., and M. C. Boyce. A three-dimensional constitutive model for the larger stretch behavior of rubber elastic materials. *J. Mech. Phys. Solids* 41:389–412, 1993.
- ³Bischoff, J. E., E. A. Arruda, and K. Grosh. A microstructurally based orthotropic hyperelastic constitutive law. *J. Appl. Mech.* 69:570–579, 2002a.
- ⁴Bischoff, J. E., E. M. Arruda, and K. Grosh. Finite element simulations of orthotropic hyperelasticity. *Finite Elem. Anal. Des.* 38:983–998, 2002b.
- ⁵Boyce, M. C., and E. M. Arruda. Constitutive models of rubber elasticity: A review. *Rubber Chem. Technol.* 73:504–523, 2000.
- ⁶Delfino, A., N. Stergiopoulos, J. E. Moore, and J. J. Meister. Residual strain effects on the stress field in a thick wall finite element model of the human carotid bifurcation. *J. Biomech.* 30:777–786, 1997.
- ⁷Drexler, E. S., C. N. McCowan, J. E. Wright, A. J. Slifka, D. D. Ivy, and R. Shandas. Comparison of strength properties of normotensive and hypertensive rat pulmonary arteries. *Biomed. Sci. Instrum.* 40:297–302, 2004.
- ⁸Flory, P. J., and J. Rehner. Statistical mechanics of cross-linked polymer networks: I. rubber elasticity. *J. Chem. Phys.* 11:512–520, 1943.
- ⁹Fung, Y. C. *Biomechanics: Mechanical Properties of Living Tissues*. New York: Springer-Verlag, 1993.
- ¹⁰Fung, Y. C., K. Fronek, and P. Patitucci. Pseudoelasticity of arteries and the choice of its mathematical expression. *Am. J. Physiol.* 237:H620–H631, 1979.
- ¹¹Hibbit, Karlsson & Sorensen, Inc. *ABAQUS/Standard Users Manual*. Version 6.4, 2003.
- ¹²Holzappel, G. A. *Nonlinear Solid Mechanics*. New York: Wiley, 2001.
- ¹³Holzappel, G. A., T. C. Gasser, and R. W. Ogden. A new constitutive framework for arterial wall mechanics and a comparative study of material models. *J. Elasticity* 61:1–48, 2000.
- ¹⁴Huang, W., Y. P. Sher, D. Delgado-West, J. T. Wu, K. Peck, and Y. C. Fung. Tissue Remodeling of rat pulmonary artery in hypoxic breathing. I. Changes of morphology, zero-stress state, and gene expression. *Ann. Biomed. Eng.* 29: 535–551, 2001a.

- ¹⁵Huang, W., D. Delgado-West, J. T. Wu, and Y. C. Fung. Tissue Remodeling of rat pulmonary artery in hypoxic breathing. II. Course of change of mechanical properties. *Ann. Biomed. Eng.* 29:552–562, 2001b.
- ¹⁶Humphrey, J. D. Mechanics of arterial wall: Review and directions. *Crit. Rev. Biomed. Eng.* 23:1–162, 1995.
- ¹⁷Humphrey, J. D. *Cardiovascular Solid Mechanics Cells Tissues, and Organs*. New York: Springer-Verlag, 2002.
- ¹⁸Hyer, M. W. *Stress Analysis of Fiber-Reinforced Composite Materials*. Ohio: The McGraw-Hill Companies, 1998, pp 151–154.
- ¹⁹Ivy, D. D. Diagnosis and management of severe pediatric pulmonary hypertension. *Cardiol. Rev.* 9:227–237, 2001.
- ²⁰James, H. M., and E. Guth. Theory of the elastic properties of rubber. *J. Chem. Phys.* 10:455–481, 1943.
- ²¹Lanning, C., S. Y. Chen, A. Hangsen, D. Chang, K. C. Chan, and R. Shandas. Dynamic three-dimensional reconstruction and modeling of cardiovascular anatomy in children with congenital heart disease using biplane angiography. *Biomed. Sci. Instrum.* 40:200–205, 2004.
- ²²Li, Y. M., M. Steffes, T. Donnelly, C. Liu, H. Fuh, J. Basgen, R. Bucala, and H. Vlassara. Prevention of cardiovascular and renal pathology of aging by the advanced glycation inhibitor aminoguanidine. *Proc. Natl. Acad. Sci. USA* 93:3902–3907, 1996.
- ²³Liu, S. Q. Alternations in structure of elastic laminae of rat pulmonary arteries in hypoxic hypertension. *J. Appl. Physiol.* 81:2147–215, 1996.
- ²⁴Meyrick, B., and L. Reid. Hypoxia-induced structural changes in the media and adventitia of the rat hilar pulmonary artery and their regression. *Am. J. Pathol.* 100:151–178, 1980.
- ²⁵Norton, G. R., J. Tsotetsi, B. Trifunovic, C. Hartford, G. P. Candy, and A. J. Woodiwiss. Myocardial collagen stiffness is attributed to alterations in cross-linked collagen rather than total collagen of phenotypes in spontaneously hypertensive rats. *Circulation* 96:1991–1998, 1997.
- ²⁶Poiani, G. J., C. A. Tozzi, S. E. Yohn, R. A. Pierce, S. A. Belsky, R. A. Berg, S. Y. Yu, S. B. Deak, and D. J. Riley. Collagen and elastin metabolism in hypertensive pulmonary arteries of rats. *Circ. Res.* 66:968–978, 1990.
- ²⁷Shandas, R., C. Weinberg, D. D. Ivy, E. Nicol, C. G. DeGroff, J. Hertzberg, and L. Valdes-Cruz. Development of a non-invasive ultrasound color M-mode means of estimating pulmonary vascular resistance in pediatric pulmonary hypertension: mathematical analysis, *in vitro* validation, and preliminary clinical studies. *Circulation* 104:908–913, 2001.
- ²⁸Susic, D., J. Varagic, J. Ahn, and E. D. Frohlich. Cardiovascular and renal effects of a collagen cross-link breaker (ALT 711) in adults and aged spontaneously hypertensive rats. *Am. J. Hypertens.* 17:328–333, 2004.
- ²⁹Takamizawa, K., and K. Hayashi. Strain energy density function and uniform strain hypothesis for arterial mechanics. *J. Biomech.* 20:7–17, 1987.
- ³⁰Vaishnav, R. N., J. T. Young, and D. J. Patel. Distribution of stresses and of strain-energy density through the wall thickness in a canine aortic segment. *Circ. Res.* 32:577–583, 1973.
- ³¹Weinberg, C., J. R. Hertzberg, D. D. Ivy, K. S. Kirby, K. C. Chan, L. M. Valdes-Cruz, and R. Shandas. Extraction of pulmonary vascular compliance, PVR and RV work from single-pressure and Doppler flow measurements in children with pulmonary hypertension—a new method for evaluating reactivity: *In vitro* and clinical studies. *Circulation* 110:2609–2617, 2004.
- ³²Wolinsky, H. Effects of hypertension and its reversal on the thoracic aorta of male and female rats. *Circ. Res.* 28:622–627, 1971.
- ³³Wuyts F. L., V. J. Vanhuyse, G. J. Langewouters, W. F. Decraemer, E. R. Raman, and S. Buyle. Elastic properties of human aortas in relations to age and atherosclerosis: a structural model. *Phys. Med. Biol.* 40:1577–1597, 1995.
- ³⁴Zhang, Y., and M. L. Dunn. Geometric and material nonlinearity during the deformation of micron-scale thin-film bilayers subject to thermal loading. *J. Mech. Phys. Solids* 52:2101–2126, 2004.